Surface-Induced Dissociation and Chemical Reactions of $C_2D_4^+$ on Stainless Steel, Carbon (HOPG), and Two Different Diamond Surfaces

Linda Feketeová,[a] Jan Žabka,[b] Fabio Zappa,[a] Verena Grill,[a] Paul Scheier,[a] Tilmann D. Märk,[a] and Zdenek Herman[a,b]

[a] Institut für Ionenphysik und Angewandte Physik, Leopold-Franzens Universität Innsbruck, Innsbruck, Austria
[b] V. Čermák Laboratory, J. Heyrovský Institute of Physical Chemistry, Academy of Sciences of the Czech Republic, Prague, Czech Republic

Surface-induced interactions of the projectile ion $C_2D_4^+$ with room-temperature (hydrocarbon covered) stainless steel, carbon highly oriented pyrolytic graphite (HOPG), and two different types of diamond surfaces (O-terminated and H-terminated) were investigated over the range of incident energies from a few eV up to 50 eV. The relative abundance of the product ions in dependence on the incident energy of the projectile ion [collision-energy resolved mass spectra, (CERMS) curves] was determined. The product ion mass spectra contained ions resulting from direct dissociation of the projectile ions, from chemical reactions with the hydrocarbons on the surface, and (to a small extent) from sputtering of the surface material. Sputtering of the surface layer by low-energy Ar^+ ions (5-400 eV) indicated the presence of hydrocarbons on all studied surfaces. The CERMS curves of the product ions were analyzed to obtain both CERMS curves for the products of direct surface-induced dissociation of the projectile ion and CERMS curves of products of surface reactions. From the former, the fraction of energy converted in the surface collision into the internal excitation of the projectile ion was estimated as 10% of the incident energy. The internal energy of the surface-excited projectile ions was very similar for all studied surfaces. The H-terminated room-temperature diamond surface differed from the other surfaces only in the fraction of product ions formed in H-atom transfer surface reactions (45% of all product ions formed versus 70% on the other surfaces). (J Am Soc Mass Spectrom 2009, 20, 927–938) © 2009 American Society for Mass Spectrometry

Over the last two decades, research on low-energy ion-surface interactions has grown substantially. Attention has been focused on selected physical and chemical processes stimulated by the impact of slow ions with incident energies up to 100 eV [1–5]. The amount of incident energy converted during these collisions into projectile internal energy is of the order of a typical chemical bond energy in molecules and thus can cause bond dissociation. As such, studies of slow ion-surface interaction can yield valuable information pertaining to the projectile or to the surface or to the nature of the ion-surface interaction.

Besides being of fundamental importance, surface interactions of molecular ions, especially of small hydrocarbon ions, are relevant for technological applications, such as plasma-wall interactions in electrical discharges and fusion plasmas [6, 7]. Hyperthermal plasma particles may collide with solid surfaces such as limiters and diverters in fusion devices, thereby eroding the material by chemical and physical processes. Charged and neutral particles emitted from the surfaces may interact with the plasma and hit the surfaces again. Hydrocarbon ions turned out to be an important component of these secondary ions. Moreover, hydrocarbons are also emitted in large quantities into the Earth's atmosphere, and some of them belong to a gaseous group known as greenhouse gases. They can be very easily ionized in the atmosphere by photoionization, and this process has been suggested as a source of energetic charged particles both in the terrestrial ionosphere and in the interstellar medium [8]. These charged particles are assumed to react on the surface of dust grains present in these media [9] and thus ion-surface interactions are of importance in this connection, too.

Reactive collisions of slow ions with surfaces have been studied in an effort to characterize molecular ions and to investigate the ion-surface interaction processes, i.e., surface-induced dissociation (SID), charge ex-

Address reprint requests to Dr. Z. Herman, J. Heyrovský Institute of Physical Chemistry, Academy of Sciences of the Czech Republic, Dolejškova 3, 18223 Prague 8, Czech Republic. E-mail: zdenek.herman@jh-inst.cas.cz

© 2009 American Society for Mass Spectrometry. Published by Elsevier Inc.
1044-0305/09/$32.00
doi:10.1016/j.jasms.2009.01.016

Published online January 31, 2009
Received November 11, 2008
Revised January 23, 2009
Accepted January 23, 2009

change reactions (CER), and surface-induced reactions (SIR). SID has been developed as an alternative tool to gas-phase collision-induced dissociations (CID) to study the fragmentation of polyatomic ions in tandem mass spectrometry [3, 4, 10–13]. Ion-surface collisions lead to a transfer of kinetic energy into the internal modes of the projectile ion, causing fragmentation that can be used to characterize the projectile ion or the surface [3, 10, 14]. The overall energy balance in an ion-surface collision can be written as

$$E_{tot} = E_{tr} + E_{int} = E'_{int} + E'_{tr} + E'_{surf} \quad (1)$$

where E_{tr} is the translational energy of the incident projectile ion, E_{int} is its initial internal energy, E'_{int} is the internal energy of the surface-excited projectile ion after the collision, E'_{tr} is its translational energy, and E'_{surf} is the energy absorbed by the surface. Over the past 15 y, several terms in eq 1 were investigated to characterize their effect on the fragmentation process of polyatomic projectile ions in surface collisions. The fraction of impact energy transformed during a surface collision into internal energy of the projectile ion was the subject of several studies for a variety of projectiles and for a number of different surfaces [3–5, 15–21].

In the current work, we have investigated two types of diamond surfaces [O(air)-terminated and H-terminated] obtained from the ρ-BeSt coating company, where a new process for manufacturing nanometer thick diamond coatings has been recently developed [22]. The H-terminated diamond surface topped with bound H atoms is expected to be hydrophobic, nonadsorbing, and nonreactive. Alternately, termination of the diamond surface with air caused bonding of the empty top bonds with oxygen or OH (N does not stick to diamond) and thus the O(air)-terminated diamond surface behaves hydrophilic.

Our interest in the present study was focused on comparison of the two different diamond surfaces with stainless steel and carbon (HOPG) surfaces. The incident ion used was the radical cation $C_2D_4^+$. The surfaces were studied at room temperature and thus one had to expect that the surfaces would be covered by a layer of hydrocarbons as shown earlier in our experiments with stainless steel [23] and HOPG [24]. The aim of this study was to find out whether the collisions of the projectile ions with HOPG and the two diamond surfaces at room temperature, the hydrophobic H-diamond and the hydrophilic O-diamond surface, would lead to different results or whether the effect of the hydrocarbon coverage would be dominant, and whether the nature of the underlying surface would affect the hydrocarbon adsorption. The earlier studied room-temperature stainless steel surface was used as a standard hydrocarbon-covered surface for comparison. The results for room-temperature HOPG surface (studied here at a different incident angle than in [24] were complemented by results on heated (600 °C) surface, where the hydrocarbon coverage was effectively removed [18, 24].

Mass spectra of product ions from collisions of molecular ions $C_2D_4^+$ with these different surfaces were investigated using two different ion-surface apparatuses in Innsbruck and in Prague. The projectile ions were produced by electron impact ionization of ethane (C_2D_6) molecules in low-pressure ion sources, their incident energy range was from a few eV to 55 eV and the incident angle was 45°. The deuterated species $C_2D_4^+$ was used to allow for distinguishing between direct fragmentation of the projectile ion, product ions resulting from chemical reactions of the projectile with the surface (reaction products), and sputtered ionic species from the surface.

Collisions of $C_2H_4^+$ with hydrocarbon covered stainless steel surface have been investigated previously in Innsbruck [23] in studies of the influence of the initial internal energy of the projectile ions on the collision energy resolved mass spectra (CERMS curves). A scattering study [24] of $C_2H_n^+$ and $C_2D_n^+$ (n = 2, 3, 4, 5) hydrocarbon ions and their interaction with heated (clean) and room-temperature (hydrocarbon covered) HOPG surfaces was carried out in Prague. In these measurements [24] the projectile ions $C_2H_4^+$ and $C_2D_4^+$ were formed by electron bombardment on ethylene molecules and the incident angle was 30 [0] (with respect to the surface). Survival probabilities of the hydrocarbon projectile ions, their fragmentation processes, and chemical reactions at the surface were determined.

Experimental

The experiments described in this study were carried out on two different ion-surface devices, one in Innsbruck and one in Prague. The compatibility of the two different machines in providing comparable mass spectra on hydrocarbon-covered surfaces was shown in earlier joint experiments [23–27]. The mass spectra of product ions from both machines showed, within the experimental error, good agreement.

Innsbruck Experiments

The relative abundance of product ions in dependence on incident projectile ion energy (CERMS curves) were measured with the tandem mass spectrometer BESTOF described in detail in our earlier papers [10, 28]. In brief, it consists of a double focusing two-sector-field mass spectrometer (reversed geometry) combined with a linear time-of-flight mass spectrometer. Projectile ions were produced in a Nier-type ion source (a commercial CH5 mass spectrometer source operated normally at pressures of about 4.10^{-6} Torr) by impact of 100 eV electrons on ethane (C_2D_6) molecules. The ions produced were extracted from the ion source region and accelerated to 3 keV for mass (and energy) analysis by the double-focusing two-sector-field mass spectrometer. After passing the mass spectrometer exit slit, the ions were refocused by an Einzel lens and decelerated to the required incident energy before interacting with

the target surface. Shielding the target area with conical shield plates minimized field penetration effects. The incident impact angle of the projectile beam was kept at 45° and the scattering angle was fixed at 46° (with respect to the surface). The incident energy of ions impacting on the surface was defined by the potential difference between the ion source and the surface. The energy spread of the primary ion beam was determined by measuring the (reflected) total ion signal as a function of surface potential. The energy spread of the primary beam of $C_2D_4^+$ was in the range of 250 to 300 meV (full-width at half-maximum). A fraction of the product ions formed at the surface exited the shielded chamber through a 1 mm diameter orifice. The ions were then subjected to a pulsed deflection-and-acceleration field that initiated the time-of-flight analysis of the ions. The second mass analyzer was a linear time-of-flight mass selector with a flight tube of about 80 cm in length. The mass selected ions were detected by a double-stage multi-channel plate, connected to a multi-channel scaler (time resolution of 10 ns per channel) and a computer. The product ion intensities were obtained by integration of the recorded signals. The surfaces with a size of $\sim 5 \times 10$ mm were polished stainless steel surface (SS), O-terminated diamond (DO), and H-terminated diamond (DH) surfaces. The diamond surfaces were attached to a surface holder, whereas the stainless steel surface formed a part of the holder. The surface holder could be rotated 360° and vertically moved to change the surface of interest. The experiments were performed at room temperature, so it was expected that surfaces would be covered by background hydrocarbons despite a surface chamber vacuum of the order of 2×10^{-9} Torr.

Prague Experiments

Mass spectra of product ions from collisions of $C_2D_4^+$ with room-temperature and heated carbon (HOPG) surfaces were measured with the Prague beam scattering apparatus EVA II modified for ion-surface collision studies. Applications of the apparatus to the surface studies was described earlier [5, 16–18, 26, 29]. In the present experiments, the projectile hydrocarbon ions were formed by bombardment with 80 eV electrons on deuterated ethane C_2D_6 in a low-pressure ion source. Ions were extracted from the ionization chamber, accelerated to about 150–200 eV, mass analyzed by a 90° permanent magnet, and decelerated to the required energy in a multi-element deceleration lens. The resulting beam of mass selected $C_2D_4^+$ ions had an energy spread of 200 meV, full-width-at-half-maximum (FWHM), angular spread of 1.6° (FWHM), and geometrical dimensions of 0.4 mm × 1.0 mm when leaving the exit slit. The beam was directed towards the carbon target surface under a pre-adjusted incident angle Φ_S = 45° (with respect to the surface, same as in the Innsbruck experiments). Ions scattered from the surface passed through a detection slit (0.4 mm × 1.0 mm) into a stopping potential energy analyzer. After energy analysis the ions were focused and accelerated to 1000 eV into a detection mass spectrometer (a magnetic sector instrument), and detected by counting the ions at the output of a Galileo channel multiplier. The primary beam exit slit, the target, and the detection slit were kept at the same potential during the experiments and this equi-potential region was carefully shielded by μ-metal sheets. The incident ion beam source-target section could be rotated about the scattering center with respect to the detection slit to obtain angular distributions. Translational energy distributions of product ions could be measured at different scattering angles. The mass spectra of product ions were recorded with the stopping potential set at zero in the maximum of the angular distribution (in the experiments reported here at the scattering angle Θ'_S = 25°, with respect to the surface).

The carbon surface target was a 5 mm × 12 mm sample of HOPG from which the surface layer was peeled off immediately before placing it into vacuum. The sample was mounted on a stainless steel holder located 10 mm in front of the exit slit of the projectile ion deceleration system. The carbon target surface kept at room temperature was covered with a layer of hydrocarbons randomly adsorbed from back-streaming rotary pump oil molecules or their fragments, as shown in our previous publications and indicated by the occurrence of H-atom transfer [16–18, 24, 26] and carbon chain build up (formation of C3 ions) reactions [18, 24]. In another set of experiments, the carbon surface was heated to 600 °C and under these conditions the concentration of hydrocarbons on the surface decreased more than 100-times, as indicated by the absence of the products of the above mentioned surface chemical reactions [18, 24] (see also results in Table 1).

Results

Collisions of $C_2D_4^+$

Mass spectra of product ions resulting from interactions of $C_2D_4^+$ with three of the investigated surfaces, SS, DO, and DH were measured on the Innsbruck machine BESTOF for several incident energies from a few eV up to at least 30 eV (in case of SS up to 55 eV) to obtain the collision energy resolved mass spectra of product ions (CERMS curves). The data are summarized in Table 1 as relative intensities of the particular ion in question (I_i) divided by the sum of all product ions (ΣI_i), i.e., as $I_i/\Sigma I_i$. The corresponding data are plotted in Figure 1a, c, d. The Innsbruck data were supplemented with mass spectra of product ions from collisions of $C_2D_4^+$ with carbon (HOPG) surface kept at room temperature and heated to 600 °C, measured on the Prague apparatus (Table 1 and Figure 1b).

The data in Table 1 and the CERMS curves in Figure 1 for collisions of $C_2D_4^+$ with room-temperature SS, diamond DO and DH, and HOPG surfaces show several similarities. The mass spectra of product ions show the presence of

Table 1. Mass spectra of product ions from surface collisions of $C_2D_4^+$ in dependence on incident energy (ion abundance in % of $I_i/\Sigma I_i$)

		Incident energy [eV]															
		$C_2D_4^+$ stainless steel surface															
m/z	Ion	2,7	5,2	6,2	7,2	8,7	10,2	12,7	15,2	17,7	20,2	25,2	30,2	35,2	40,2	45,2	55,2
15	CDH^+											0,9	0,5	1,4	1,5	2	2,6
16	CD_2^+											1	1,1	1	2	2,2	2,3
17	CD_2H^+											1,4	1,9	1,9	2,2	2,1	1,8
18	CD_3^+											1,1	1,2	1,3	1,3	0,8	0,8
27	$C_2D_2H^+$									1,2	1,8	3,7	6,3	9,2	10,3	13,2	15,6
28	$C_2D_2^+$			1,5	3,2	8,8	14,2	14,6	16	13,3	11,8	11,7	11,3	12,5	13,2	14,4	12,6
29	$C_2D_2H^+$				1	2,1	5,8	13,9	20,6	27,4	28,2	29,5	23,7	23,1	18,9	17,3	16,3
30	$C_2D_3^+$			0,9	1,6	6	10,1	15,1	24,3	28,9	33	29,8	26,5	21,1	19,1	14,1	8,5
32	$C_2D_4^+$	100	99	96,1	91,8	77,2	59,3	39,1	20,4	15,1	8,2	3	1,4	0,9			>
33	$C_2D_4H^+$		1	1,6	2,5	5,8	10,5	9,8	8,1	4	2,6	1,2	0,3	0,4			
39	$C_3H_3^+$										0,5	1,6	2,6	3,1	3,6	5,3	7
40	$C_3DH_2^+/C_3H_4^+$								1	1,7	1,2	1,4	4,2	4,3	4,5	4,9	5
41	$C_3D_2H^+/C_3H_5^+$							1,5	2,6	2,7	5,4	5,4	8,9	8,5	10,9	10,7	12,1
42	$C_3D_3^+/C_3H_6^+$							1,2	2,1	1,1	1,5	2,2	2,3	2,9	2,1	2,7	2,9
43	$C_3D_2H_3^+/C_3H_7^+$							1,8	2,5	2,3	2,5	2,3	3,5	4	5	4,6	5,7
44	$C_3D_3H_2^+$							1,9	1,5	1,5	1,4	0,9	1,2	0,6	1,3	1	1,1
45	$C_3D_4H^+$							1,1	1	0,8	0,7	0,8	0,5	1	1,1	1	1,3
55*	$C_4D_xH_y^+$										0,7	1,7	1,2	1,1	1,3	2	2,4
57*	$C_4D_xH_y^+$										0,6	0,5	1,4	1,6	1,8	1,8	2,1
*x = 0–4; y = 1, 3, 5, 7, 9.																	
		$C_2D_4^+$ diamond-oxygen surface															
m/z	Ion		3.4		6,4	8,4	9,4	10,4	12,4	15,4	20,4	25,4	30,4				
27	C_2DH^+										1,9	5,1	6,2				
28	$C_2D_2^+$					8	11,2	12,6	18,7	18,6	18,1	15,9	14,9				
29	$C_2D_2H^+$							7,5	15,4	20	25,3	26,5	24,2				
30	$C_2D_3^+$						2,8	8,9	18,2	25,2	30	31,5	29				
32	$C_2D_4^+$		100		100	92	79,8	60,6	31,4	13,8	5,8	2,9	1,6				
33	$C_2D_4H^+$						6,2	10,4	16,3	10,2	4,2	0,9					
40	$C_3DH_2^+/C_3H_4^+$									2	2,7	3,6	5				
41	$C_3D_2H^+/C_3H_5^+$									2,2	2,8	5,5	9,2				
42	$C_3D_3^+/C_3H_6^+$									2,8	2,5	2,2	3,5				
43	$C_3D_2H_3^+/C_3H_7^+$									1,7	4,4	4	4,6				
44	$C_3D_3H_2^+$									3,4	2,3	1,9	1,8				
		$C_2D_4^+$ diamond-hydrogen surface															
m/z	Ion	3.3		6,3	8,3	9,3	10,3	11,3	12,8	14,3	16,3	18	20,3	25,3	30,3		
27	C_2DH^+													3,9	4		
28	$C_2D_2^+$				0,7	1,2	2	3,8	6,8	9,7	17,1	21,5	21,4	20,7	21,4		
29	$C_2D_2H^+$									2,7	7	8,8	12,4	15,2	16,3		
30	$C_2D_3^+$					0,3	0,9	1,4	3,7	8,4	15,6	20,7	32,9	35,9	35,2		
32	$C_2D_4^+$	100		100	99,3	98,5	97,1	94,4	88,6	78,1	58,4	46,6	22,6	7,6	6,7		
33	$C_2D_4H^+$							0,4	0,9	1,1	1,9	2,4	3,1	2,7			
40	$C_3DH_2^+/C_3H_4^+$												1,2	1,9	3,3		
41	$C_3D_2H^+/C_3H_5^+$												1,5	3,7	5,1		
42	$C_3D_3^+/C_3H_6^+$												1,3	2,4	2,6		
43	$C_3D_2H_3^+/C_3H_7^+$												2,2	4,5	3,9		
44	$C_3D_3H_2^+$												1,3	1,7	1,6		
		$C_2D_4^+$ carbon (HOPG) surface (room temperature and heated)															
m/z	Ion		6.5		8.5		9.5		10.5		12.5		16.3		31.3		46.3
		Room temperature surface															
27	C_2DH^+								1.1		2.0				5.5		10.4
28	$C_2D_2^+$		1.7		4.3		15.1		11.4		19.6		15.1		13.2		19.7
29	$C_2D_2H^+$				10.9		11.0		23.9		20.4		23.5		26.0		21.4
30	$C_2D_3^+$		1.0		6.5		15.1		1'8.2		27.3		32.2		32.2		22.1
32	$C_2D_4^+$		97.3		64.3		48.6		38.1		22.4		12.2		1.0		0.4
33	$C_2D_4H^+$				11.9		10.3		7.4		8.2		6.2				

(Continued)

Table 1. Continued

		Incident energy [eV]		
39	$C_3H_3^+$		3.2	4.5
40	$C_3DH_2^+/C_3H_4^+$	0.8	3.0	4.2
41	$C_3D_2H^+/C_3H_5^+$	4.9	6.0	8.8
42	$C_3D_3^+/C_3H_6^+$	2.4	1.6	2.6
43	$C_3D_2H_3^+/C_3H_7^+$	0.6	1.1	1.6
	Heated surface			
28	$C_2D_2^+$	35.1	18.6	22.6
30	C_2D_3	42.6	78.7	77.4
32	$C_2D_4^+$	22.3	2.7	0

1. Undissociated projectile ions $C_2D_4^+$ (*m/z* 32), the relative concentration of which decreases with increasing incident energy from 100% at very low incident energies to less than a few % above 20 eV (with the exception of the DH surface);
2. Fragment ions at *m/z* 30 ($C_2D_3^+$), 28 ($C_2D_2^+$), and a small amount at *m/z* 16 (CD_2^+); these product ions are formed by simple direct dissociations of the surface-excited projectile ions and the main dissociation pathways are

$$C_2D_4^+ \rightarrow C_2D_3^+ + D \quad (2a)$$

$$C_2D_4^+ \rightarrow C_2D_2^+ + D_2 \quad (2b)$$

$$C_2D_4^+ \rightarrow CD_2^+ + CD_2 \quad (2c)$$

As reported earlier [2, 3, 15] and shown in our previous papers [16–18, 24, 26], the fragmentation of the surface-excited polyatomic projectile ion occurs after the interaction with the surface in a unimolecular way. The relative abundances of these ions include statistical contributions from reactive processes (see the next point);

3. Fragment ions C2 and C1 at odd masses *m/z* 33, 29, 27, 15; these ions contain one hydrogen atom from the surface hydrocarbons and are formed in chemical reactions of H-atom transfer between the projectile ion and hydrocarbons on the room-temperature surfaces (H-S) and decay via unimolecular dissociation reactions of the excited $C_2D_4H^+$ ion formed, as discussed in detail earlier [24, 30]. The main dissociation pathways are

$$C_2D_4^+ + H\text{-}S \rightarrow C_2D_4H^+ + \text{-}S \quad (3a)$$

$$C_2D_4H^+ \rightarrow C_2D_2H^+(C_2D_3^+) + D_2(HD) \quad (3b)$$

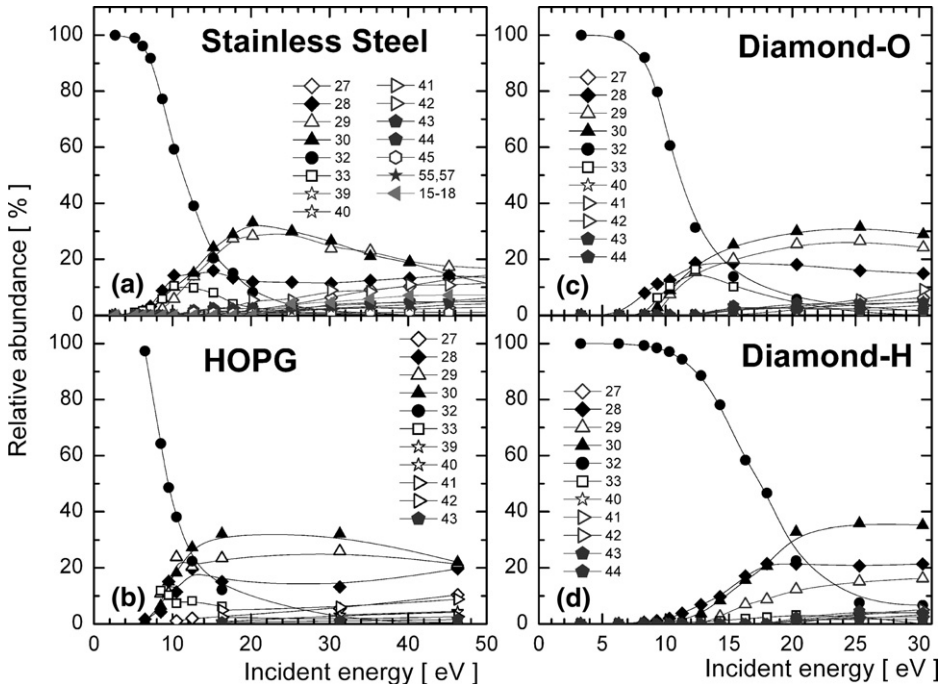

Figure 1. CERMS curves of product ions from collisions of $C_2D_4^+$ with room-temperature surfaces of (**a**) stainless steel, (**b**) carbon (HOPG), (**c**) diamond-O, (**d**) diamond-H.

$$C_2D_4H^+ \rightarrow CDH^+(CD_2^+) + CD_3(CD_2H) \quad (3c)$$

The C_2DH^+ fragment ion observed is most probably formed via further dissociation of $C_2D_2H^+$ to $C_2DH^+ + D$ in a process with a rather high activation energy (see also later on CERMS curves for neat reaction products); the pathway $C_2D_4H^+ \rightarrow C_2D_3H^+ + D \rightarrow C_2DH^+ + D_2 (+D)$ does not seem probable due to practical absence of *m/z* 31 ($C_2D_3H^+$) in the mass spectra. The fragmentation of these reaction products contributes statistically [24, 30] to the abundance of product ions at even masses ($C_2D_3^+$, $C_2D_2^+$, CD_2^+).

4. Product ions $C_3X_n^+$ (*n* = H, D) at *m/z* 39–44; these products are a mixture of pure surface-sputtered hydrocarbon ions and carbon-chain build-up chemical reactions between the projectile ions and terminal CH_2^- groups of the surface hydrocarbon, as discussed in detail in our previous paper [24].

However, there are also differences in the spectra and CERMS curves for the four investigated surfaces. The main difference is that in case of the room-temperature DH surface the relative abundance of the incident ion $C_2D_4^+$ is considerably larger at higher incident energies than for the other surfaces. While the CERMS curve for $C_2D_4^+$ (*m/z* 32) decreases to 50% at incident energies 10–11 eV for the SS, DO, and HOPG surfaces, for the DH surface it reaches 50% only at 17–18 eV, and at 25–30 eV the fraction of $C_2D_4^+$ is higher (7%–8%) than for the other three surfaces (less than 3%). The increased amount of the nondissociated incident ion in interactions with the DH surface, in comparison with the other surfaces, may seem to imply a lower incident-to-internal energy transfer for collisions with the DH surface than with the other three surfaces.

Collisions of Ar^+

We used the technique of sputtering as a tool to see differences or similarities of the SS, DO, and DH surfaces at room temperature. Sputtering of ions is the basis of secondary ion mass spectrometry (SIMS), a standard method in surface studies [1, 31]. More recently, sputtering by Cs^+ ion of keV energies has been used successfully to characterize soft-landed biomolecular ions [32, 33].

In our experiments, an intense Ar^+ ion beam of incident energy from tens to 400 eV made it possible to reach the level of physical sputtering and to detect the secondary ion mass spectra of the sputtered ions. The mass spectra of the sputtered ions are summarized in Table 2 for incident energies up to 75 eV and for higher incident energy of 400 eV.

The respective CERMS curves of the sputtered ions (including the incident Ar^+ ions) are summarized in a simplified form in Figure 2. The points represent the sum of $C_nH_x^+$ (where *n* = 1, 2, 3, 4, and 6) ions in the same *n*-group, i.e., "26–29" is the sum of the relative abundances for product ions of *m/z* = 26, 27, 28, and 29. The product ions with relative abundance lower than 2.5% over the whole incident energy range were not

Table 2. Dominant scattered product ions from surface collisions of Ar^+ with stainless steel, diamond–oxygen and diamond–hydrogen surfaces in dependence on incident energy (ion abundance in % of $I_i/\Sigma I_i$–relative abundance). Relative abundance of dominant product ions of every C_n group (with the highest abundance) is bolded

Range of incident energies	C_n group of hydrocarbons	*m/z*	Surface		
			Stainless steel	Diamond–oxygen (air)	Diamond–hydrogen
Up to 75 eV	C_2H_x	27	**25**	20	**18**
		28		**33**	7
		29	**25**	20	10
	C_3H_x	39	**15**	10	8
		41	**15**	**15**	
		43	10	**15**	**25**
		45			8
	C_4H_x	55	3	4	
		57	4	4	
	C_6H_x	72		5	
		73	5	**10**	**15**
		74			4
400 eV	Physically sputtered product ions	15		9	20
		28		**63**	**55**
		29		21	24
		30		6	
		23	31		
		39	**33**		
		40	5		
		52	6		
		56	9		

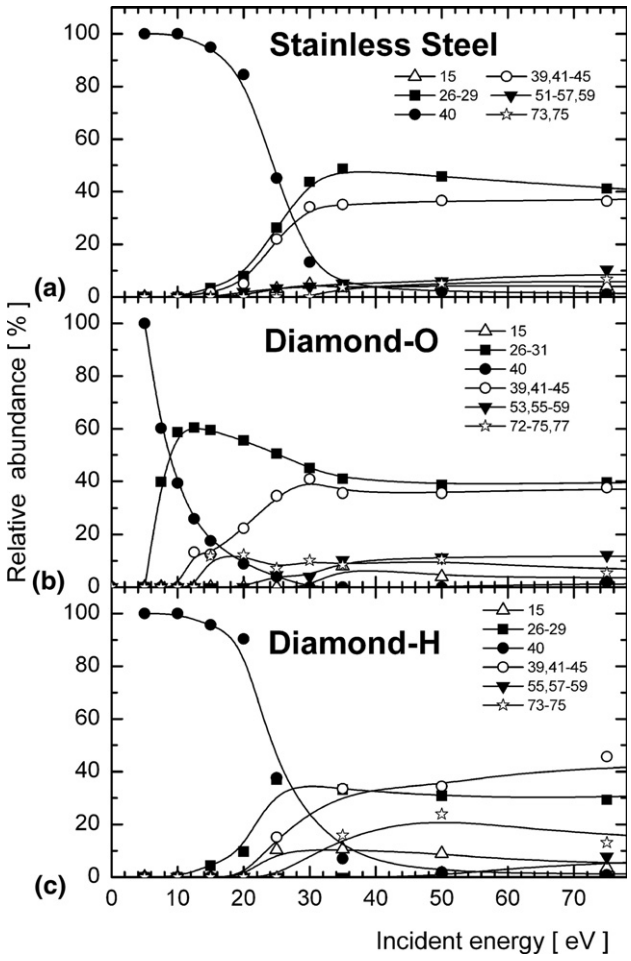

Figure 2. CERMS curves of product ions form sputtering by Ar^+ ions of room-temperature surfaces of (**a**) stainless steel, (**b**) diamond-O, (**c**) diamond-H.

included in Table 2. The C5 group of hydrocarbons has not been observed in any spectra.

The CERMS curves for all three investigated surfaces show similarities in relative abundance of C2 and C3 hydrocarbon ions (about 40% at incident energies above 40 eV), only for the DH surface the abundance of C2 ions seems to be somewhat lower (30%). A significant difference is a sudden increase of the C2 group on the DO surface at low incident energies between 5 and 30 eV. A closer inspection shows that this increase is due to a specific increase of *m/z* 28 in this region. This ion is most probably the sputtered CO^+ ion and may indicate the presence of larger amounts of oxidized carbon compounds on the DO surface, in comparison with other investigated surfaces. The presence of the oxidized compounds (ketones, alcohols) as well as the increased abundance of the C6 group hydrocarbon ions (aromatic hydrocarbons) in the spectra with DO and DH surfaces may reflect the history of preparation of these surfaces.

In comparing CERMS curves in Figures 1 and 2, one has to take into consideration that the absolute survival probability of Ar^+ ions on a hydrocarbon-covered room-temperature HOPG surface is only 0.005% [34], while that of $C_2D_4^+$ ion is about 1% [24], i.e., 200-times larger. Assuming that the sputtering efficiency of low-energy Ar^+ and $C_2D_4^+$ are comparable, the relative abundance scale in Figure 2 (relative to the Ar^+ projectile) must be reduced 200 times to fit the relative abundance scale in Figure 1 (related to the $C_2D_4^+$ projectile). Thus, the sputtered ions of relative abundances of tens of percents in Figure 2 represent less than 1% in the relative abundance scale of Figure 1. Similar conclusions on the relative role of sputtered ions can be obtained from data on CD_4^+ collisions with room-temperature HOPG surfaces [18].

Data Analysis and Discussion

Direct Dissociative Processes

The measured abundance of the product ions from collisions of the projectile ion with different surfaces contains contributions from two major surface processes: ions from direct dissociative processes of the surface-excited projectile ion and ions from surface chemical reaction of H-atom transfer (including their dissociation products). To separate the two contributions, the relative intensities of the product ions containing an H-atom (odd masses of *m/z* 33, 29, 27, and 15) and the statistical contributions of these reaction products to even masses (to *m/z* 30, 28, 16) were subtracted from the ion abundances as given in Table 1 and Figure 1. The resulting product ion intensities, relevant to the direct dissociative process, were re-normalized and the resulting relative ion abundances $(I_i)_D/\Sigma(I_i)_D$ were plotted in Figure 3 as a function of the incident energy. The error bars represent statistical errors in measured ion count rates. The resulting CERMS curves for product ions from the direct dissociative processes show three major product ions, the non-dissociated projectile ion $C_2D_4^+$ and two fragment ions, $C_2D_3^+$ and $C_2D_2^+$. The relative abundance of CD_2^+, observed only with SS surfaces, was lower than 1% and was neglected in the analysis.

The CERMS curves for direct dissociation on different surfaces shown in Figure 3 are very similar for SS, DO, and HOPG, but those for the DH surface differ from them. For this surface the relative abundance of the undissociated projectile decreases more slowly with incident energy and extends to considerable higher E_{inc}. This increased relative abundance of the undissociated projectile ion seems to imply a less efficient (lower) translational-to-internal energy-transfer in collisions with the DH surface. A plot of the ratio of relative abundances of $[C_2D_4^+]/[C_2D_2^+]$, the ratio of *m/z* 32/28, (Figure 4a) shows, within the experimental error, a good agreement for the surfaces SS, HOPG, and DO, but the ratio increases considerably more steeply with decreasing E_{inc} for the DH surface. On the other hand, a plot of the relative abundance of the fragment ions $[C_2D_2^+]/[C_2D_3^+]$, the ratio of *m/z* 28/30, (Figure 4b) is very similar for all surfaces, including the DH surface.

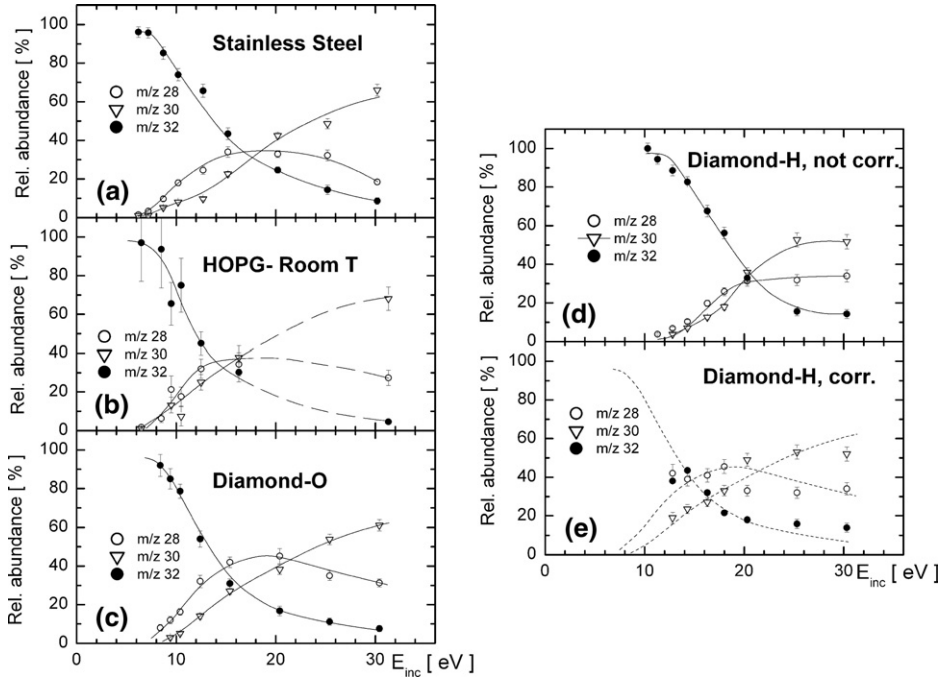

Figure 3. CERMS curves of product ions from direct dissociative processes of $C_2D_4^+$ on surfaces of (**a**) stainless steel; (**b**) carbon (HOPG); (**c**) diamond-O; (**d**) diamond-H (uncorrected); (**e**) diamond-H (corrected, see text).

This is a contradiction: if the DH surface differs from the other surfaces in that the incident translational-to-internal energy-transfer is lower, as the increased abundance of the undissociated projectile seems to imply, the difference should be reflected not only in the different ratio of *m/z* 32/28, but also in a difference in the ratio of *m/z* 28/30. The relative abundance of all three ions in the break-down pattern of the $C_2D_4^+$ ion [35] (see Figure 5a and the next section) changes sufficiently fast with increasing internal energy to expect that both the ratio of *m/z* 32/28 and of *m/z* 28/30 should be different for the DH surface. This contradiction suggests that the measured abundance of the undissociated projectile ion $C_2D_4^+$ (*m/z* 32) for the DH surface contains an interfering contribution that does not result from investigated inelastic surface collisions. In our previous papers [16–18, 24, 30], we observed that the abundance of the projectile ion in the mass spectra of product ions may have two components (sometimes of comparable size): a part of abundance due to inelastically scattered undissociated projectile ion from surface collisions, and a part due to projectile ions deflected with full incident energy in front of the surface by surface charges without making a collision with the surface. The latter contribution artificially increases the intensity of the projectile ions. This contribution of deflected projectile ions was observed to increase with decreasing incident energy and with increasing intensity of the projectile ion beam, though the phenomenon was not investigated quantitatively in detail. This interfering component of the projectile ion abundance can be easily identified in the Prague experiments, where the translational energy of the product ions can be measured, and the Prague data (Table 1, Figure 1b, HOPG surface) were corrected by subtracting it, if necessary, from the $C_2D_4^+$ (*m/z* 32) abundance. However, in the Innsbruck experiments, where only the relative abundance of product ions can be measured without energy analysis, this correction is not possible. The projectile ion intensities in the Innsbruck experiments are at least by an order of magnitude lower than in the Prague experiments and the phenomenon of surface charges presumably plays usually a minor role. A good agreement between (corrected) Prague data for HOPG and Innsbruck data for SS and DO surfaces, as indicated by data in Figure 4, confirms this assumption. However, the DH surface is reported to have a low electrical conductivity [22] and the phenomenon of surface charges may play a much more important role. An unsuccessful experiment in Prague appears to confirm this: a preliminary study of $C_2D_4^+$ collisions with the DH surface under Prague experimental conditions (a much stronger projectile ion beam than in Innsbruck experiments) showed practically only deflected projectile ions with fragmentation processes reduced to a very small contribution.

This reasoning led us to the conclusion that the abundance of the undissociated projectile ions $C_2D_4^+$ (*m/z* 32) from the Innsbruck DH experiments in Figures 1 and 3 has to be corrected for an interfering contribution of the deflected ions. This correction was made by multiplying, at different incident energies, the relative abundance of *m/z* 32 in Figure 3d (DH surface) by the ratio of the $C_2D_4^+$ abundance from Figure 4 for the SS,

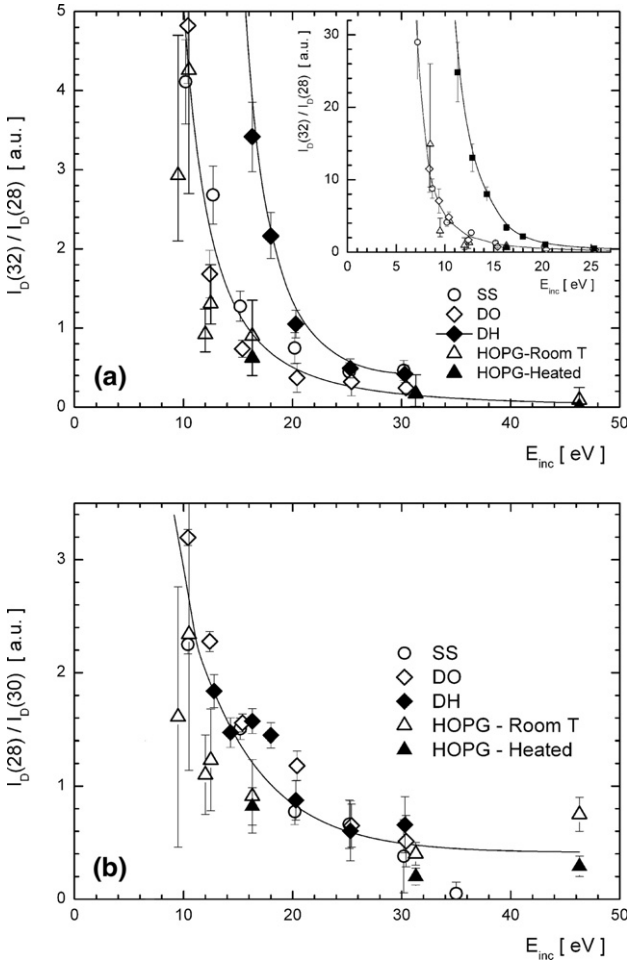

Figure 4. (**a**) The ratio of ion abundance $C_2D_4^+/C_2D_2^+$ (*m/z* 32/28) from direct dissociative processes of $C_2D_4^+$ as a function of the incident energy for different surfaces. (**b**) The ratio of ion abundance of fragment ions $C_2D_2^+/C_2D_3^+$ (*m/z* 28/30) from direct dissociative processes of $C_2D_4^+$ as a function of the incident energy for different surfaces.

DO, and HOPG surfaces to the $C_2D_4^+$ abundance for the DH surface. After renormalization with these corrected values of $C_2D_4^+$, the corrected CERMS curves for the DH surface (Figure 3e) resemble very much the CERMS curves for the other surfaces (SS, HOPG, OD). The dashed lines drawn in Figure 3e are in fact the CERMS curves for the DO surface, as given in Figure 3c, and they fit the corrected data for the DH surface quite well. Thus, one can say that the increased abundance of the projectile ions in the CERMS curves from experiments with the DH surface, in comparison with the other surfaces (SS, HOPG, DO) is not due to a different energy-transfer in the surface collisions, but rather to an interfering contribution from projectile ions deflected in front of the surface by surface charges.

In conclusion, the CERMS curves of product ions of direct dissociation processes from collisions of $C_2D_4^+$ with four different surfaces kept at room temperature (SS, HOPG, DO, corrected DH) now look very similar, and this implies a very similar energy transfer in ion-surface collisions. This similarity is evidently caused by the hydrocarbon layer that covers at room temperature all these surfaces, as evidenced by the Ar^+ sputtering experiments and by the occurrence of H-atom transfer reactions in collisions of $C_2D_4^+$ with these surfaces. The nature of the underlying surface plays, in this respect, an insignificant role.

Estimation of the Internal Energy of the Surface-Excited Projectile Ions $C_2D_4^+$

Internal energy of ions activated in surface collisions can be determined by various methods. The "thermometer molecule method" developed by Cooks and collaborators uses consecutive fragmentation processes of molecules like methylcarbonyls [3, 36], other methods use the extent of fragmentation of the incident ion in combination with the known break-down pattern of it [37]. In our estimation of the internal energy of $C_2D_4^+$ excited in surface collisions, we used the CERMS curves for the direct dissociative processes (Figure 3) and followed the procedure used in our previous papers [5,

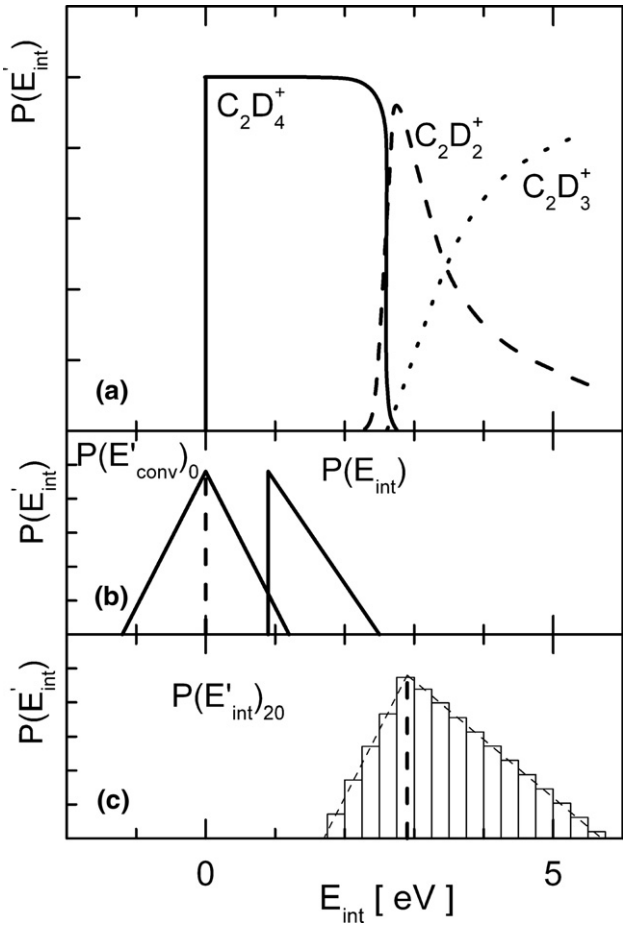

Figure 5. (**a**) Break-down pattern of $C_2D_4^+$ [35]; (**b**) distribution functions for translational-to-internal energy-transfer, $P(E'_{conv})_0$ and initial internal energy of $C_2D_4^+$, $P(E_{int})$; (**c**) example of the internal energy distribution of the surface-excited projectile ion $C_2D_4^+$, $P(E'_{int})$, at the collision energy of 20 eV.

16, 18, 29]. This procedure is based on using different forms of energy-transfer distributions together with the breakdown pattern of the incident ion in question, trying to find the best fit with the relative abundance of the product ions in the mass spectrum of the surface-excited ions at different incident energies. The breakdown pattern of $C_2D_4^+$, the dependence of the relative abundances of molecular and fragment ions on the internal energy of the molecular ion, is well known, and the most reliable data come from threshold photoelectron photoion coincidence (TPEPICO) experiments [35] (Figure 5a).

In case of the $C_2D_4^+$ projectile ion the estimation of this energy-transfer is a more complicated procedure than in our previous studies because the initial internal energy of the projectile ion, $E_{int}(C_2D_4^+)$, formed from C_2D_6 in the low-pressure Nier-type ion source, is rather large [23] and cannot be neglected in the overall energy balance. This additional energy has to be added to the energy converted from translational to internal energy in the surface collision, E'_{conv}, which changes with the incident energy. The initial internal energy distribution, $P(E_{int})$, was estimated for $C_2H_4^+$ formed from C_2H_6 in our previous paper [23], where it was also shown that this initial internal energy is fully available as an additional energy component in the surface-induced dissociation processes. A simplified form of $P(E_{int})$ of $C_2H_4^+$, as derived in reference [23], has a triangular form, starting at 0.9 eV and decreasing linearly to 2.5 eV (see Figure 5b).

For the shape of the distribution of energy converted in the surface collision from incident translational energy to internal energy, $P(E'_{conv})_0$, we chose a simplified form based on the widths of the earlier determined distributions on hydrocarbon-covered surfaces [5, 16, 18, 29]. This shape was approximated by a triangular distribution with the total width of ±1.2 eV (see Figure 5b).

Using $P(E'_{conv})_0$, $P(E_{int})$, and different fractions of incident translational energy of the projectile ions, we obtained the best fit over a wide range of incident energy, E_{tr}, for the distribution of the internal energy of the projectile ion excited in the surface collision, $P(E'_{int})$, (see eq1) in the form

$$P(E'_{int}) = 0.10\ E_{tr}\ P(E'_{conv})_0 + P(E_{int}) \quad (4)$$

An example of $P(E'_{int})$ used in the calculation of the ion abundances at the incident energy of 20 eV, $P(E'_{int})_{20}$, is shown in Figure 5c. The agreement between experimental and calculated abundances of ions for the direct dissociation CERMS curves was good over the range of incident energies 11–30 eV, as shown in comparison with the experimental (SS and DO surfaces) and calculated spectra in Table 3. Thus, the fraction of translational energy converted into internal energy, derived for collisions of $C_2D_4^+$ with the above studied different surfaces at room temperature, is 10% of the incident translational energy, somewhat larger than the often quoted value [5, 16, 20, 29] of about 6%. However, the present case is more complicated because the final internal energy of the surface-excited projectile ion, $P(E'_{int})$, is composed of two components of comparable magnitude, the initial internal energy of the projectile ion, $P(E_{int})$ and the component from net conversion of translational-to internal energy in the surface collision, $P(E'_{conv})$.

It is worth noting that attempts to calculate abundances of product ions from direct dissociation processes with uncorrected CERMS curves for the DH surface (Figure 3d), using different incident-to-internal distribution functions (from $0.04E_{tr}$ to $0.10E_{tr}$) did not lead to consistent results.

Reactive Processes

The above mentioned separation of the relative abundances of product ions from collisions of $C_2D_4^+$ with different surfaces into a part due to direct dissociative processes and a part due to reactive processes at the surface makes it possible to investigate in more detail the reactive processes and to assess the ratio of surface reactive versus surface dissociative and reactive processes as a function of the incident energy of the projectile ions.

The dependence of the relative abundance of product ions formed in reactive processes on the incident energy, the CERMS curves of the product ions from reactive processes, are shown in Figure 6a for collisions of $C_2D_4^+$ with DO and DH surfaces. These curves were obtained from data in Table 1 as the relative intensity of $C_2X_5^+$ (X = H,D) at *m/z* 33 ($C_2D_4H^+$), $C_2X_3^+$ (sum of intensities at *m/z* 29 and the respective statistical contribution to *m/z* 30), and $C_2X_2^+$ (sum of intensities at *m/z* 27 and the respective statistical contribution to *m/z* 28). The CERMS curves show that the abundance of the primary product formed in the H-atom transfer surface reaction (3a), $C_2D_4H^+$ ($C_2X_5^+$ in Figure 6a) decreases with increas-

Table 3. Comparison of experimental and calculated ion abundances for the direct fragmentation of the projectile ion $C_2D_4^+$ incident on stainless steel (SS) and diamond-O (DO) surfaces as a function of incident energy

		Incident energy [eV]														
		11			16			20			25			30		
m/z	Ion	SS	DO	calc	SS	DO	calc	SS	DO	calc	SS	DO	calc	SS	DO	calc
28	$C_2D_2^+$	22	22	22	35	42	40	33	44.2	43.1	33.0	35.0	42.7	25.4	31.3	36.5
30	$C_2D_3^+$	10	10	15	28	28	29	42.5	38.3	38.6	52.6	53.8	49.1	66	61.1	62.4
32	$C_2D_4^+$	71	72	63	37	30	31	24.5	17.5	18.3	14.4	11.2	8.2	8.6	7.6	1.0

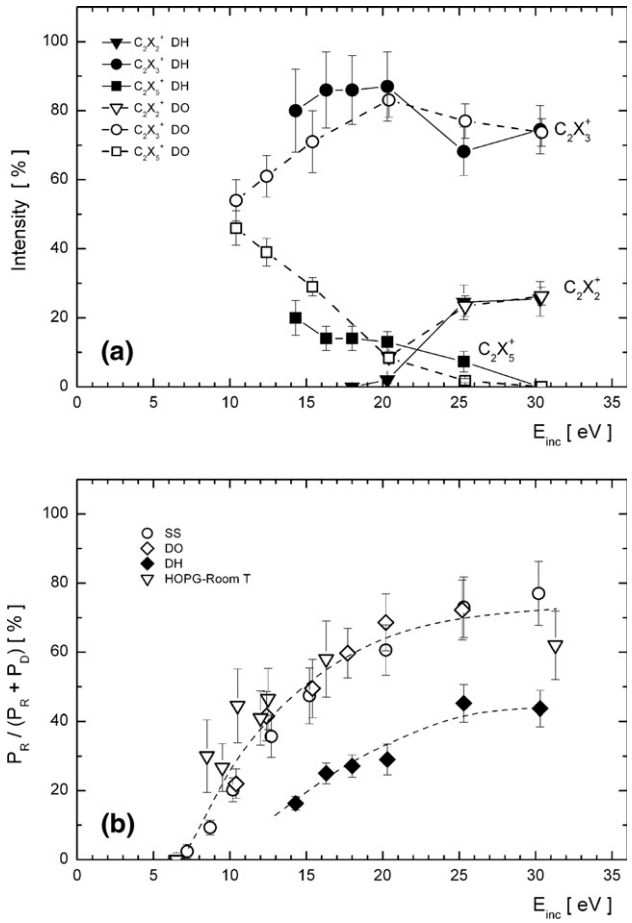

Figure 6. (**a**) CERMS curves for product ions from surface chemical reactions from collisions of $C_2D_4^+$ with room-temperature diamond-O and diamond-H surfaces. (**b**) Probability of reactive processes versus the sum of reactive process and direct dissociative processes, $P(R)/P(R) + P(D)$, as a function of incident energy of $C_2D_4^+$ on room-temperature surfaces of stainless-steel, carbon (HOPG), diamond-O, and diamond-H.

ing incident energy and gives rise to fragmentation products $C_2X_3^+$ (reaction 3b) and $C_2X_2^+$. The threshold for $C_2X_2^+$ formation is rather high (about 20 eV) and thus it supports the above mentioned assumption that this fragment is formed by further dissociation of the fragment $C_2X_3^+$. The CERMS curves for DO and DH surfaces agree reasonably well and this provides further support for the conclusion that the energy-transfer on both surfaces is similar.

Finally, the separation of the data in Table 1 to abundances of product ions from direct dissociative processes and from surface reaction processes made it possible to estimate the relative ratio of both processes at different collision energies. The data were obtained by summing in Table 1 the relative abundances of product ions at *m/z* 27–33 related to these two groups of processes. The results are given in Figure 6b for all four surfaces investigated (SS, HOPG, DO, and DH) as the relative probability of surface reaction, P(R), to the sum of both, probability of direct dissociation and surface reaction, P(D) + P(R). It can be seen that the ratio P(R)/P(R) + P(D) increases from a threshold between 6–7 eV to about 70% at the incident energy of 25–30 eV for the SS, HOPG, and DO surfaces. The increase for the DH surface is smaller, reaching about 45%.

The threshold of 6–7 eV for the surface reaction of H-atom transfer between $C_2D_4^+$ and surface hydrocarbons was observed earlier [38]. It is worth mentioning that the gas-phase reaction between the ethylene cation and C4–C8 saturated hydrocarbons

$$C_2H_4^+ + H\text{-}R \rightarrow C_2H_5^+ + R \quad (5)$$

is slightly endoergic by about 0.4 eV. With the above estimated 10% translational-to-internal energy conversion in the surface collision this leads to an expected threshold at about 4 eV, in a reasonable agreement with the observed value of 6–7 eV. The lower probability of reactive processes, P(R)/P(R) + P(D), on the DH surface may be connected with a stronger bonding of hydrocarbons to this surface as suggested by higher thresholds for sputtering of C2 and C3 hydrocarbons by Ar^+ ions (Figure 2), in comparison with the DO surface.

Conclusions

1. Interaction of the projectile ion $C_2D_4^+$ with four different surfaces (stainless steel, carbon-HOPG, diamond-O, and diamond-H) kept at room temperature (hydrocarbon covered) was studied to investigate the influence of different surfaces, underlying the hydrocarbon coverage, on the fragmentation and the chemical reactions at surfaces. Mass spectra of the product ions were measured over the range of incident energies from a few eV up to about 50 eV and the respective CERMS curves of the product ions were determined.
2. The product ions observed with projectile ions $C_2D_4^+$ indicated both fragmentation of the projectile ion $C_2D_4^+$, chemical reactions of H-atom transfer with the surface hydrocarbons, chemical reactions of carbon chain build up (C3 hydrocarbon ion formation), and a small contribution of hydrocarbon ions sputtered from the surface. Sputtering by Ar^+ ions showed the presence of hydrocarbons on all investigated surfaces.
3. The CERMS curves of the product ions were analyzed to provide the CERMS curves for product ions coming from direct surface-induced dissociation of the projectile ion and those coming from chemical reactions of H-atom transfer.
4. The CERMS curves for direct dissociation of the projectile were (after a correction of the data for the DH surface) very similar for all studied surfaces and thus indicated a similar translational-to-internal energy transfer in the surface collisions. No substantial difference was found between the two room-temperature (hydrocarbon covered) substances of diamond (DO and DH).

5. The product ion distributions over the studied incident energy range could be fitted by an energy-transfer distribution function that included the initial internal energy of the projectile ion and assumed a conversion of 10% of the incident energy of the projectile ion in the surface translation-to internal energy-transfer.
6. The CERMS curve for reactive processes (formation and fragmentation of $C_2D_4H^+$) on DO and DH surfaces were very similar. The only observed difference between the two diamond surfaces at room temperature was the ratio of probabilities of reactive versus reactive and dissociative processes as a function of incident energy. This ratio increased from a threshold at 6–7 eV to about 70% for the SS, HOPG, and DO surfaces, but only to about 45% for the DH surface.

Acknowledgments

The authors acknowledge that this work, supported by the European Communities under the Contracts of Association between EURATOM and ÖAW and EURATOM and IPP.CR, was carried out within the framework of the European Fusion Development Agreement (EFDA). The views and opinions expressed herein do not necessarily reflect those of the European Commission. The research was partly supported by FWF, Wien. The authors thank ρ-BeSt Coating for providing the diamond samples used in this work. Postdoctoral fellowship grant from Brazilian agency CNPq is gratefully acknowledged (F.Z.).

References

1. Low Energy Ion-Surface Interactions; Rabalais, J. W., Ed.; J. Wiley: New York, 1994.
2. Niehus, H.; Heiland, W.; Taglauer, H. Low-Energy Ion Scattering at Surfaces. *Surf. Sci. Reports* **1993,** *17,* 213–303.
3. Cooks, R. G.; Ast, T.; Mabud, M. D. Collisions of Polyatomic Ions with Surfaces. *Int. J. Mass Spectrom.* **1990,** *100,* 209–265.
4. Grill, V.; Shen, J.; Evans, C.; Cooks, R. G. Collisions of Ions with Surfaces at Chemically Relevant Energies: Instrumentation and Phenomena. *Rev. Sci. Instrum.* **2001,** *72,* 3149.–3179.
5. Herman, Z. Collisions of Slow Polyatomic Ions with Surfaces: The Scattering Method and Results. *J. Am. Soc. Mass Spectrom.* **2003,** *14,* 1360–1372.
6. Hofer, W. O.; Roth, J. Physical Processes of the Interaction of Fusion Plasmas with Solids; Academic Press: San Diego, CA, 1996.
7. Atomic and Molecular Processes in Fusion Edge Plasma; Janev, R. K., Ed.; Plenum: New York, 1995.
8. Leach, S. The formation and Destruction of Doubly-Charged PAH Cations in the Interstellar Medium. *J. Electron Spectrosc. Relat. Phenom.* **1986,** *41,* 427–438.
9. Hewitt, C. N. Reactive Hydrocarbons in the Atmosphere; Academic Press: San Diego, 1999.
10. Mair, C.; Fiegele, T.; Biasioli, F.; Wörgötter, R.; Grill, V.; Lezius, M.; Märk, T. D. Surface-Induced Reactions of Polyatomic Ions and Cluster Ions: Insight into Plasma-Surface Interactions. *Plasma Source Sci. Technol.* **1999,** *8,* 191–199.
11. Wörgötter, R.; Mair, C.; Fiegele, T.; Grill, V.; Märk, T. D.; Schwarz, H. Characterization of Hydrocarbon Cluster Ion Products by Surface Induced Reactions. *Int. J. Mass Spectrom. Ion Processes* **1997,** *164,* L1.
12. Hanley, L. Polyatomic Ion-Surface Interactions. *Int. J. Mass Spectrom. Ion Processes* **1998,** *174,* 1–328.
13. Herman, Z. Surface Collisions of Small Cluster Ions at Incident Energies $10–10^2$ eV. *Int. J. Mass Spectrom.* **2004,** *233,* 361–371.
14. Hayward, M. J.; Mabud, M. A.; Cooks, R. G. Ion/Surface Collisions for Distinction of Isomeric $C_6H_6^+$ and $C_6H_6^{2+}$ Ions. *J. Am. Chem. Soc.* **1988,** *110,* 1343–1346.
15. Wysocki, V. H.; Kenttämaa, H. I.; Cooks, R. G. Internal Energy Distributions of Isolated Ions after Activation by Various Methods. *Int. J. Mass Spectrom. Ion Processes* **1987,** *75,* 181–208.
16. Kubišta, J.; Dolejšek, Z.; Herman, Z. Energy Partitioning in Collisions of Slow Polyatomic Ions with Surfaces: Ethanol Molecular Ions on Stainless Steel Surfaces. *Eur. Mass Spectrom.* **1998,** *4,* 311–319.
17. Žabka, J.; Dolejšek, Z.; Roithová, J.; Grill, V.; Märk, T. D.; Herman, Z. Energy Partitioning in Collisions of Slow Polyatomic Ions with Carbon Surfaces. *Int. J. Mass Spectrom.* **2002,** *213,* 145–156.
18. Roithová, J.; Žabka, J.; Dolejšek, Z.; Herman, Z. Collisions of Slow Polyatomic Ions with Surfaces: Dissociation and Chemical Reactions of CD_5^+, CD_4^+, and CD_3^+, and their Isotopic Variants on Room-Temperature and Heated Carbon Surfaces. *J. Phys. Chem. B* **2002,** *120,* 8293–8301.
19. Beck, R. D.; Rockenberger, J.; Weis, P.; Kappes, M. M. Fragmentation of C_{60}^+ and Higher Fullerenes by Surface Impact. *J. Chem. Phys.* **1996,** *104,* 3638–3650.
20. Biasioli, F.; Fiegele, T.; Mair, C.; Herman, Z.; Echt, O.; Aumayr, F.; Winter, H.-P.; Märk, T. D. Surface-Induced Dissociation of Singly- and Multiply-Charged Fullerene Ions. *J. Chem. Phys.* **2000,** *113,* 5053–5057.
21. Burroughs, J. A.; Wainhaus, S. B.; Hanley, L. Impulsive Excitation of $FeCP_2^+$ and $SiMe_3^+$ During Surface-Induced Dissociation of Organic Multilayers. *J. Chem. Phys.* **1995,** *103,* 6706–6715.
22. http://www.rhobest.com.
23. Qayyum, A.; Herman, Z.; Tepnual, T.; Mair, C.; Matt-Leubner, S.; Scheier, P.; Märk, T. D. Surface-Induced Dissociation of Polyatomic Projectile Ions with Different Initial Internal Energy Content. *J. Phys. Chem.* **2004,** *108,* 1–8.
24. Jašík, J.; Žabka, J.; Feketeová, L.; Ipolyi, I.; Märk, T. D.; Herman, Z. Collisions of Slow Polyatomic Ions with Surfaces: Dissociation and Chemical Reactions of $C_2H_2^+$, $C_2H_3^+$, $C_2H_4^+$, $C_2H_5^+$, and their Deuterated Variants $C_2D_2^+$ and $C_2D_4^+$ on Room-Temperature and Heated Carbon Surfaces. *J. Phys. Chem. A* **2005,** *109,* 10208–10215.
25. Wörgötter, R.; Kubišta, J.; Žabka, J.; Dolejšek, Z.; Märk, T. D.; Herman, Z. Surface-Induced Reactions and Decomposition of the Benzene Molecular Ion $C_6H_6^+$: Product Ion Intensities, Angular and Translational Energy Distributions. *Int. J. Mass Spectrom. Ion Processes* **1998,** *174,* 53–62.
26. J. Jašík, J. Roithová, J. Žabka, A. Pysanenko, L. Feketeová, I. Ipolyi, T. D. Märk, Z. Herman: Surface-Induced Dissociation of Dications and Cations: Collisions of Dications $C_7H_8^{2+}$, $C_7H_7^{2+}$, and $C_7H_6^{2+}$, and a Comparison with the Respective Cations $C_7H_8^+$ and $C_7H_7^+$. *Int. J. Mass Spectrom.* **2006,** *249/250,* 162–170.
27. L. Feketeová, T. Tepnual, V. Grill, P. Scheier, J. Roithová, Z. Herman, T. D. Märk:Surface-Induced Dissociation and Reactions of Cations and Dications $C_7H_8^{+/2+}$, $C_7H_7^{+/2+}$, and $C_7H_6^{2+}$: Dependence of Mass Spectra of Product Ions on Incident Energy of the Projectiles. *Int. J. Mass Spectrom.* **2007,** *265,* 337–346.
28. Mair, C.; Fiegele, T.; Biasioli, F.; Herman, Z.; Märk, T. D. Surface-Induced Reactions of Acetone Cluster Ions. *J. Chem. Phys.* **1999,** *111,* 2770–2778.
29. Žabka, J.; Dolejšek, Z.; Herman, Z. Energy Partitioning in Collisions of Slow Polyatomic Ions with Surfaces: Ethanol Molecular Ions on Surfaces Covered by Self-Assembled Monolayers (CF-SAM, CH-SAM, COOH-SAM). *J. Phys. Chem. A* **2002,** *106,* 10861–10869.
30. Pysanenko, A.; Žabka, J.; Märk, T. D.; Herman, Z. Collisions of Slow Hydrocarbon Ions CD_4^+, CD_5^+, $C_2D_4^+$, and $C_2H_5^+$ with Room-Temperature and Heated Tungsten Surfaces. *Int. J. Mass Spectrom.* **2008,** *277,* 229–235.
31. Bennighoven, A.; Rüdenager, F. G.; Werner, H. W. *Secondary Ion Mass Spectrometry*; J. Wiley: New York, 1987.
32. Alvarez, J.; Cooks. R. G.; Barlow, S. E.; Gaspar, D. J.; Futrell, J. H.; Laskin, J. Preparation and In Situ Characterization of Surfaces Using Soft Landing in a Fourier Transform Ion Cyclotron Resonance Mass Spectrometer. *Anal. Chem.* **2005,** *77,* 3452–3460.
33. Hadjar, O.; Futrell, J. H.; Laskin, J. First Observation of Charge Reduction and Desorption Kinetics of Multiply Protonated Peptides Soft-Landed onto Self-Assembled Monolayer Surfaces. *J. Phys. Chem. C* **2007,** *111,* 18220–18225.
34. Pysanenko, A.; Žabka, J.; Feketeova, L.; Mark, T. D.; Herman, Z. Collisions of Slow Ions C3 with Room Temperature Carbon Surfaces: Mass Spectra of Product Ions and the Ion Survival Probability, *Eur. J. Mass Spectrom.* **2008,** *14,* 345–343.
35. Stockbauer, R.; Inghram, M. G. Threshold Photoelectron-Photoion Coincidence Mass Spectrometric Study of Ethylene and Ethylene-d_4. *J. Chem. Phys.* **1975,** *62,* 4862–4870.
36. Cooks, R. G.; Ast. T.; Predeep, T.; Wysocki, V. H. Reactions of Ions with Organic Surfaces. *Acc. Chem. Res.* **1994,** *27,* 316–323.
37. Vékey, K.; Somogyi, A.; Wysocki, V. H. Internal Energy Distribution of Benzene Molecular ions in Surface-Induced Dissociation. *J. Mass Spectrom.* **1995,** *30,* 212–217.
38. Pysanenko, A.; Žabka, J.; Herman, Z. Scattering of Low Energy (5-12 eV) $C_2D_4^+$ Ions from Room-Temperature Carbon Surfaces. *Collect. Czech Chem. Commun.* **2008,** *73,* 755–770.